

1 **Dependence of sub-hourly solar variability statistics on time interval and cloud**
2 **vertical position**

3 Mónica Zamora Zapata¹ and Jan Kleissl²

4 ¹*Departamento de Ingeniería Mecánica, Universidad de Chile*

5 ²*Department of Mechanical and Aerospace Engineering, University of California San*
6 *Diego*

7 (*mzamora@uchile.cl.)

8 (Dated: 13 June 2022)

9 Solar variability corresponds to strong variations of the solar irradiance, caused mainly by
10 the presence of clouds. Practical uses of solar resource data, such as the design of pho-
11 tovoltaic solar plants, usually employs several years of hourly data, neglecting subhourly
12 features. The effect of clouds on short-time variability can differ by cloud type, suggesting
13 that some cloud effects could be ignored when working with hourly data. In this work, we
14 study compare statistics of solar variability calculated at different time intervals, and sepa-
15 rate the analysis by cloud categories. We use 1 minute solar data and cloud radar products
16 from the ARM CACTI campaign in Córdoba, Argentina, where a wide variety of clouds
17 exist. We classify the clouds based on their vertical position and observe solar variability
18 using the mean and standard deviation of the clear sky index for varying time intervals of 5,
19 15, 30, and 60 minutes. Time intervals affect the mean and standard deviation of the clear
20 sky index differently for each cloud type: longer time intervals neglect small variability
21 and overestimate the mean clear sky index of low and mid clouds, while high clouds do
22 not change as much. The effect is also palpable when measuring ramps: the percentile 95
23 of the ramps obtained for 1 minute is 21 times greater compared to 1 hour. This ratio varies
24 per cloud type, with the strongest differences occurring for mid clouds, having ramps that
25 are 73 times stronger.

26 I. INTRODUCTION

27 The inherent variability of the solar resource is a big challenge for increasing renewable energy
28 penetration in the electric grid¹. Variability can occur at different timescales: seasonal changes,
29 diurnal changes, or at very short timescales of minutes or seconds². In the PV industry, historical
30 hourly data is typically used to design a plant, meaning that the variability at the longer timescales
31 is captured and that the behavior at shorter timescales is usually neglected. Short term variability
32 matters both at a local scale, affecting the performance of electrical equipment, and at a global
33 scale, affecting the electric grid's balance and economic dispatch when using hourly schedules³,
34 which makes variability a challenge for increasing PV penetration.

35 Quick changes in the solar resource are mainly caused by passing clouds. 'A cloud can di-
36 minish the solar irradiance that reaches the surface, or it can also augment in a process known
37 as cloud enhancement, which occurs by forward scattering through thin clouds or on the sides
38 of clouds^{4,5}. The resulting variability is a compound effect of the optical properties of the cloud
39 field, its spatial organization, its motion in space, as well as its own dynamics. Different types of
40 clouds have distinct ways of evolving: some move with the wind without changing much, while
41 others can either rise and grow, or dissipate in the span of an hour. Each location in the world
42 has meteorological conditions that favor the existence of some clouds during the year, resulting
43 in unique climatological records of cloudiness, thus of solar variability. Learning how each cloud
44 type affects solar variability can facilitate a systematic analysis of cloud effects and expand it to
45 other locations.

46 Previous works have studied the link between solar variability and cloud type. Hinkelman
47 et al.⁶ characterized solar ramps –the change of solar irradiance over a time interval– per cloud
48 type. They used 1 min solar irradiance data from the SURFRAD network (continental US), and
49 GOES satellite images with 30 min and 4 km spatial resolution to distinguish 12 cloud categories.
50 They found that the features of the ramps are characteristic for each cloud type, leading to overall
51 differences in each site due to the different frequency that they can display. Reno et al.⁷ used
52 a GOES satellite product (GSIP) with 6 cloud types and hourly resolution, and 1-minute solar
53 irradiance for 2 sites in the US, creating hourly statistics of average and standard deviation of the
54 clear sky index. They found that different cloud types correspond to distinct variability features
55 and ramp rates. Lohmann et al.⁸ characterized solar variability not only in time but also in space
56 using a network of sensors in Germany, and classified sky conditions as clear, overcast or mixed

57 using the average and standard deviation of the clear sky index. They found that mixed conditions
58 were linked to more variability and stronger ramps.

59 The aforementioned studies have similar conclusions but since the cloud classes differ, it is hard
60 to compare the results in a quantitative way. Satellite products have improved but their weakest
61 feature is resolution both in time and space; therefore, they prevent us from having more detailed
62 information on local cloud features. Ground-based methods for observing cloud properties also
63 exist, including derived products from sky imagers, ceilometers, radars, and lidar. Currently, one
64 of the most complete products can be obtained from radars, as they have great time resolution and
65 can distinguish different layers of clouds. Very recent work has used these type of products to
66 demonstrate improvements in solar variability forecasts⁹, with not much attention given to time
67 resolution issue. Thus, exploring both satellite and ground products is important to complement
68 our understanding of the link between cloud types and solar variability.

69 The present work explores the dependence of the calculation of statistics of solar variability to
70 time intervals and cloud types, using 1 minute resolution data. The high temporal resolution will
71 allow us to determine the impact of neglecting sub-hourly features. The data is from the ARM
72 CACTI campaign in Argentina, where a wide variety of clouds exist. The paper is structured as
73 follows: Section II describes the data and methods to calculate solar variability and the cloud
74 classification, Section III presents the main findings and analyzes the effect of time resolution, and
75 Section IV contains the conclusions.

76 **II. DATA AND METHODS**

77 **A. Data**

78 We use data from the mobile ARM CACTI (Cloud, Aerosol, and Complex Terrain Interactions)
79 campaign in Córdoba, Argentina (32,12 °S, 64.73° W) which was deployed during 2018-2019.
80 This location was chosen by ARM due to its unique features, which display a large variety of
81 cloud types: “orographic boundary layer clouds, deep convection, and some mesoscale systems
82 uniquely observable from a single fixed site”¹⁰. The unique variety of cloud conditions makes it
83 interesting not only for atmospheric research but also for studies on solar variability.

84 For the solar resource, we retrieve the global horizontal irradiance (GHI) from the surface
85 radiation product QCRAD1LONG¹¹, which is available at 1 min resolution from 2018/9/23 to

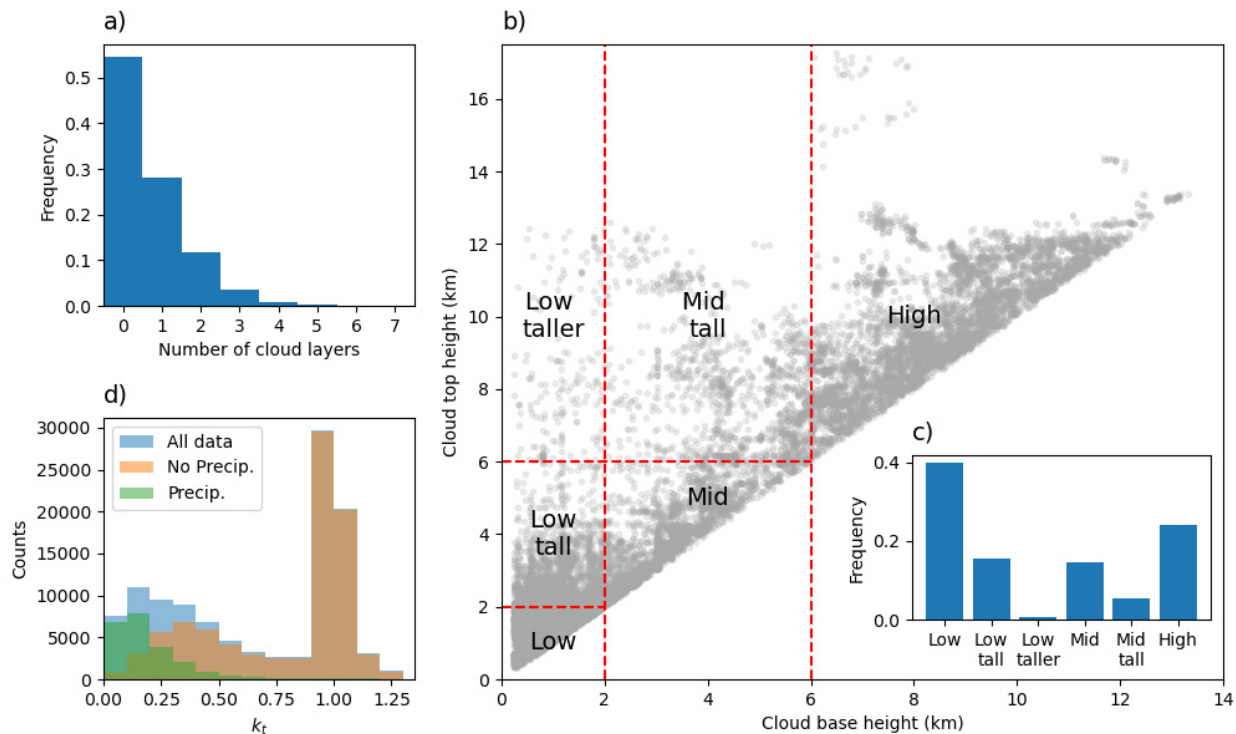


FIG. 1. Statistics of the dataset and cloud classification scheme: a) histogram of the number of cloud layers, with a maximum of 7, b) cloud base and top heights of the observations of single cloud layers (gray points), with a visualization of the cloud classification (dashed red lines), c) histogram of cloud types, and d) the histogram of the clear sky index k_t (ratio between measured and clear sky global horizontal irradiance), emphasizing the effect of the cases labeled as precipitating events.

86 2019/5/1. For the cloud properties, we use the ARSCLKAZRBND1KOLLIAS product, derived
 87 from radar and micropulse lidar results¹², which can recognize up to 10 layers of clouds, detect-
 88 ing base and top heights with a resolution of 4 s. Due to the mismatch in time resolution, we
 89 downsample the cloud data to 1 minute using the nearest reading available.

90 B. Cloud classification

91 For each time, there can be a number of cloud layers. Fig. 1a shows the histogram of the
 92 number of cloud layers present for the times considered in the study, where clear sky conditions
 93 and single cloud layers dominate.

94 The cases with a single cloud layer are classified into 6 categories based on its cloud vertical
 95 position (Fig. 1b). Both cloud base and vertical extent are considered: low, low tall, and low taller

96 all have cloud base heights lower than 2 km but the latter 2 have top heights greater than 2 or 6
 97 km, respectively. Similarly, mid and mid tall clouds have cloud base heights lower than 6 km but
 98 the latter has top heights greater than 6 km. Finally, high clouds correspond to cloud base heights
 99 greater than 6 km. Fig. 1c shows that the least common type are low taller clouds, which could
 100 correspond to extremely tall convective clouds like cumulonimbus. In this work, the classification
 101 is restricted to single cloud layers as they are the most common in this dataset and because multiple
 102 layers pose a greater challenge for a systematic analysis.

103 Precipitation events can lead to incorrect readings of cloud base heights. Measured precipitation
 104 rates are available for this site but at an hourly rate which is not useful for our sub-hourly analysis.
 105 Therefore, we discard all events with readings of cloud base heights at the surface level. Even
 106 though this selection may also leave fog events out, we do not expect their exclusion to impact our
 107 results greatly. Fig. 1d shows the histogram for k_t , where the events labeled as precipitation have
 108 a very low k_t , indicating that they may indeed correspond to thick precipitating clouds.

109 C. Clear sky index and rolling statistics

110 We use the implementation of the Perez clear sky model in pvlib^{13,14} to obtain a clear sky
 111 irradiance GHI_{cs} . We then compute the clear sky index $k_t = \text{GHI}/\text{GHI}_{cs}$. Daily values of Linke
 112 turbidity are found iteratively by finding a value that sets the clear sky index closer to 1 for the
 113 clear portions of the day.

114 Due to errors in the clear sky model near sunrise and sunset, when the irradiance is low, k_t can
 115 reach unrealistically high values. Therefore, we exclude the times with solar elevation lower than
 116 20° , which is a common practice¹⁵. In our case, while this results in an estimated loss of 20%
 117 of the daytime data, there are still more than 6 hours available for a day in May, and since the
 118 removed hours are associated with lower energy generation their impact is not significant.

119 Since the dataset has 1 minute resolution, we are able to compute rolling statistics of k_t^2 for
 120 longer time intervals (Δt) of 5, 15, 30, and 60 min. We note that there is no resampling, meaning
 121 that all calculations use the 1 minute data. The average clear sky index, \bar{k}_t , and its standard
 122 deviation, σ_{k_t} , are calculated at the center of each time interval Δt with a trapezoidal method, as

$$123 \quad \bar{k}_{t,i}(\Delta t) = \frac{1}{\Delta t} \sum_{j=i-n/2+1}^{i+n/2} \frac{k_{t,j-1} + k_{t,j}}{2} \delta t, \text{ and} \quad (1)$$

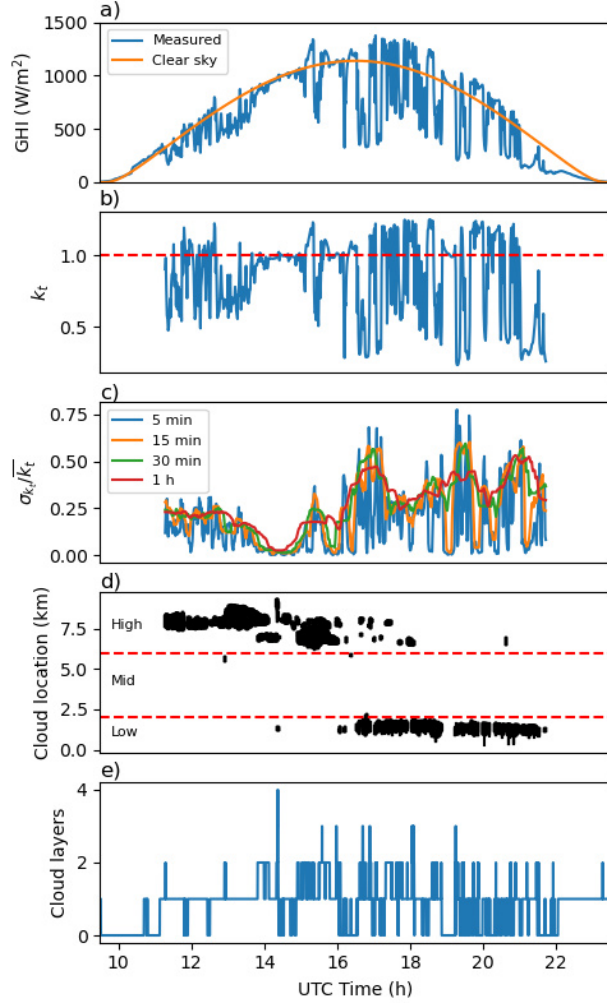


FIG. 2. Time series for January 21, 2019: a) measured and clear sky GHI at 1 min resolution, b) instantaneous clear sky index, c) normalized standard deviation of the clear sky index for different time intervals, d) the vertical position of passing clouds (shaded areas cover cloud base to cloud top heights), and e) number of cloud layers. Note that data with elevation greater than 20° has been omitted in b,c, and d).

124

$$\sigma_{k_t,i}^2(\Delta t) = \frac{1}{\Delta t^2} \sum_{j=i-n/2+1}^{i+n/2} \frac{1}{2} \left((k_{t,j-1} - \bar{k}_{t,j-1}(\Delta t))^2 + (k_{t,j} - \bar{k}_{t,j}(\Delta t))^2 \right) \delta t, \quad (2)$$

126 where i is the discrete time index, δt is the data time resolution, and $n = \Delta t / \delta t$.

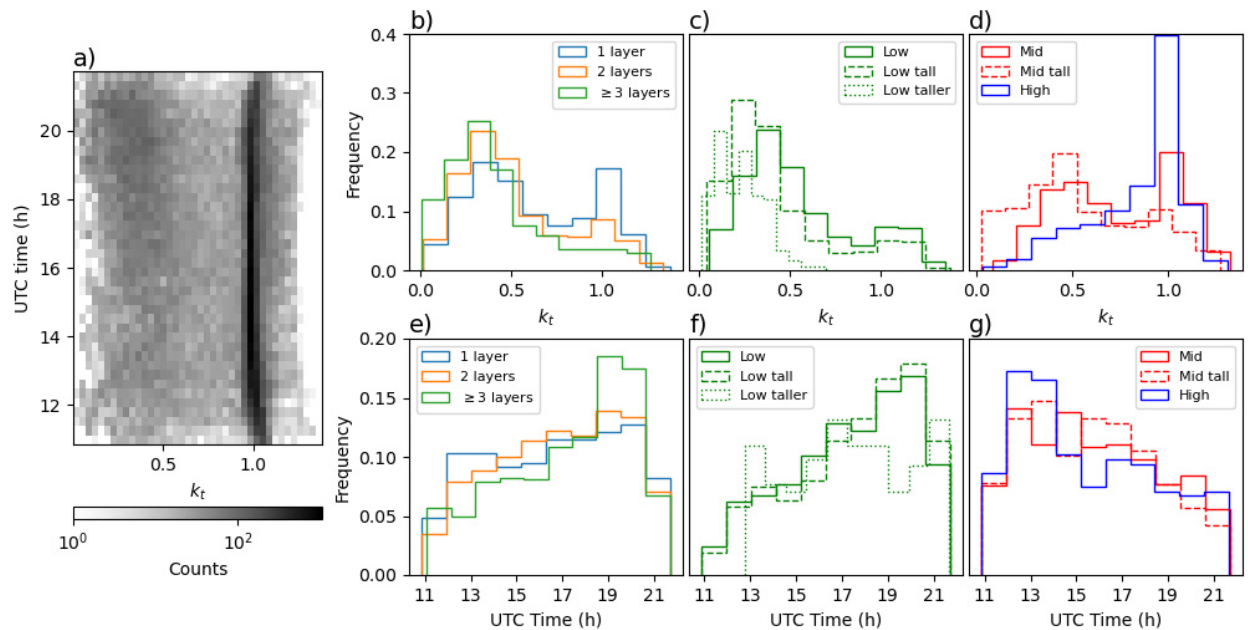


FIG. 3. Overall clear sky index statistics: a) shows the distribution of k_t over time in the day. The distribution of k_t and time in the day is then separated per number of cloud layers (b,e), and by cloud categories (c,d,f,g).

127 III. RESULTS

128 A. Sample day readings

129 Fig. 2 shows the solar and cloud readings for January 21, 2019. This day had high clouds
 130 passing in the morning and low clouds in the afternoon, with up to 4 layers of clouds, and no
 131 precipitation (Fig. 2d,e). In this case, there is a noticeable difference: low clouds induce a stronger
 132 variability than high clouds. This effect is evident in Fig. 2a,b,c, with the normalized standard
 133 deviation σ_{k_t}/\bar{k}_t being higher in the afternoon for all the time intervals considered. There is also
 134 a time window of nearly clear sky situations ($k_t \approx 1$) around 14:00 UTC, which corresponds to a
 135 period of scattered and presumably optically thinner high clouds (Fig. 2d).

136 B. Overview of site conditions

137 The observed distribution of k_t at the site is bimodal (Fig. 1d), with a predominance of near
 138 clear conditions ($k_t \approx 1$). This is also evidenced in Fig. 1a, where a 55% of the times correspond to
 139 cloudless sky conditions. Regarding the number of cloud layers, a single layer is the most common
 140 (28.1%), followed by two (11.8%); three or more layers are less frequent (5.5%). Based on the

141 cloud classification performed for the cases with a single cloud layer (Fig. 1b,c), low clouds had
 142 the highest frequency (39.8%), followed by high (23.9%), low tall (15.5%), mid (14.6%), mid tall
 143 (5.3%), and, lastly, low taller clouds (<1%).

144 Fig. 3a shows the distribution of k_t as a function of UTC time, with the counts in a logarithmic
 145 scale due to the frequent clear or near-clear sky conditions found in this dataset. For early mornings
 146 and late afternoons we see a slight increase of k_t , related to the errors that occur near sunrise and
 147 sunset, which were the reason to exclude lower elevation angles. There is a darker patch of lower k_t
 148 in the evening hours meaning that there are more clouds impacting solar radiation in the afternoon
 149 than in the morning. We can further explore these features by looking at the statistics of only
 150 cloudy events.

151 Fig. 3b,e shows the histograms of k_t and UTC time, respectively, for cloudy events and by
 152 the number of cloud layers. Only single cloud layers show a bimodal distribution for k_t , 2 layers
 153 or more display lower values of k_t . In terms of time, 3 or more layers are much more frequent
 154 in the evening, while 1 and 2 layers show a slightly flatter distribution along the day but still an
 155 increasing frequency with time in the day.

156 Finally, we can look the effect that each cloud type has on k_t and their frequency throughout
 157 the day (Fig. 3c,d,f,g). The highest values of k_t are linked mostly to high clouds and to some
 158 mid clouds. Mid tall and all low cloud types generally display lower values of k_t , with low taller
 159 clouds exhibiting the lowest k_t . The strong difference between low and high clouds is expected
 160 since the latter are often optically thinner¹⁶. High clouds are more frequent in the morning, while
 161 low and low tall clouds are more frequent in the evening, which could be a sign of them being
 162 surface-driven convective clouds such as Cumulus, which tend to develop in the afternoon when
 163 the surface heating is stronger. Low taller clouds seem to have a uniform distribution (but note the
 164 low number of samples), while mid and mid tall clouds are more frequent in the late morning and
 165 early afternoon.

166 C. Solar variability and time intervals

167 The variability measure σ_{k_t} depends on the time interval considered. We will analyze this
 168 dependence first by looking at the overall relationship between σ_{k_t} and \bar{k}_t , and then separating the
 169 analysis by cloud category.

170 Fig. 4 shows the overall effect of the time interval on the joint distribution of \bar{k}_t and σ_{k_t} .

Dependence of sub-hourly solar variability statistics on time interval and cloud vertical position

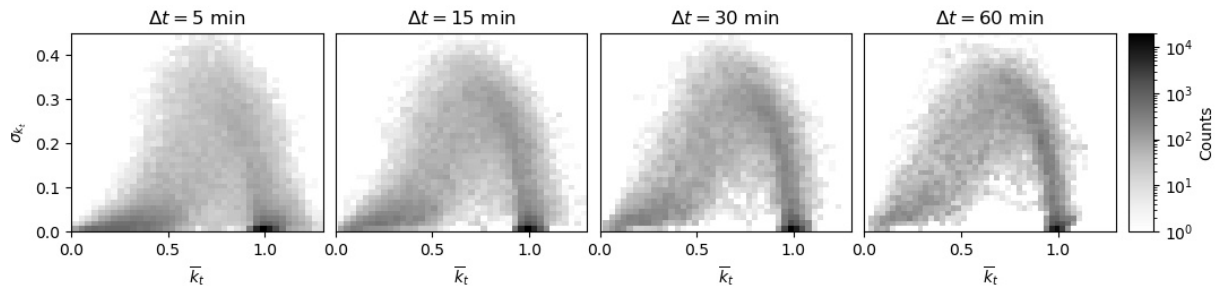


FIG. 4. Joint distribution of the clear sky index mean, \bar{k}_t , and standard deviation, σ_{k_t} , for different time intervals, Δt .

171 The time interval has a profound effect on both the mean and standard deviation of k_t : longer time
 172 windows diminish the maximum values, and by smoothing out the temporal scales, a more defined
 173 pattern is seen in the parameter space. In other words, some information is lost: by comparing the
 174 5 and 60 minute statistics, the latter misses the concentration of events linked to small \bar{k}_t and σ_{k_t} ,
 175 overestimating solar variability, finding more moments close to clear sky instances ($\bar{k}_t \approx 1$), and
 176 completely missing events with middle values of \bar{k}_t and low σ_{k_t} . While the effect is progressive
 177 with time interval, the differences between distributions are minor for 30 and 60 min. This solar
 178 variability conclusions are valid only for the site considered since the frequency of certain cloud
 179 types and clear days may affect different ranges of \bar{k}_t and σ_{k_t} .

180 We now separate the analysis, observing the time interval effect for each cloud category. Fig.
 181 5 shows the joint distributions of \bar{k}_t and σ_{k_t} per cloud type and time window. First of all, statistics
 182 for the low taller clouds are included for completeness but the low number of samples does not
 183 give statistically significant results.

184 The segregated analysis allows confirming that different cloud types occupy different regions
 185 of the parameter space. When looking at 5 min statistics, low and low tall clouds have a stronger
 186 presence in the left bottom region with lower clear sky index and lower variability. The distribution
 187 progressively changes with greater time interval, reducing the frequency of cases with short term
 188 variability. While the maximum frequency stays within that region for 15 and 30 min statistics, it
 189 is lost for the 60 min case, resulting in a more uniform distribution of \bar{k}_t and σ_{k_t} . For high clouds,
 190 the 5 min statistics shows a stronger presence at the right bottom corner, with low variability and
 191 $\bar{k}_t \approx 1$. Longer time windows increase the cases with more variability, likely through including the
 192 effect of nearby minutes. Overall, the distribution of high clouds is less affected by time interval,
 193 which confirms the tendency to be more spatially uniform. Lastly, mid and mid tall clouds occupy

Dependence of sub-hourly solar variability statistics on time interval and cloud vertical position

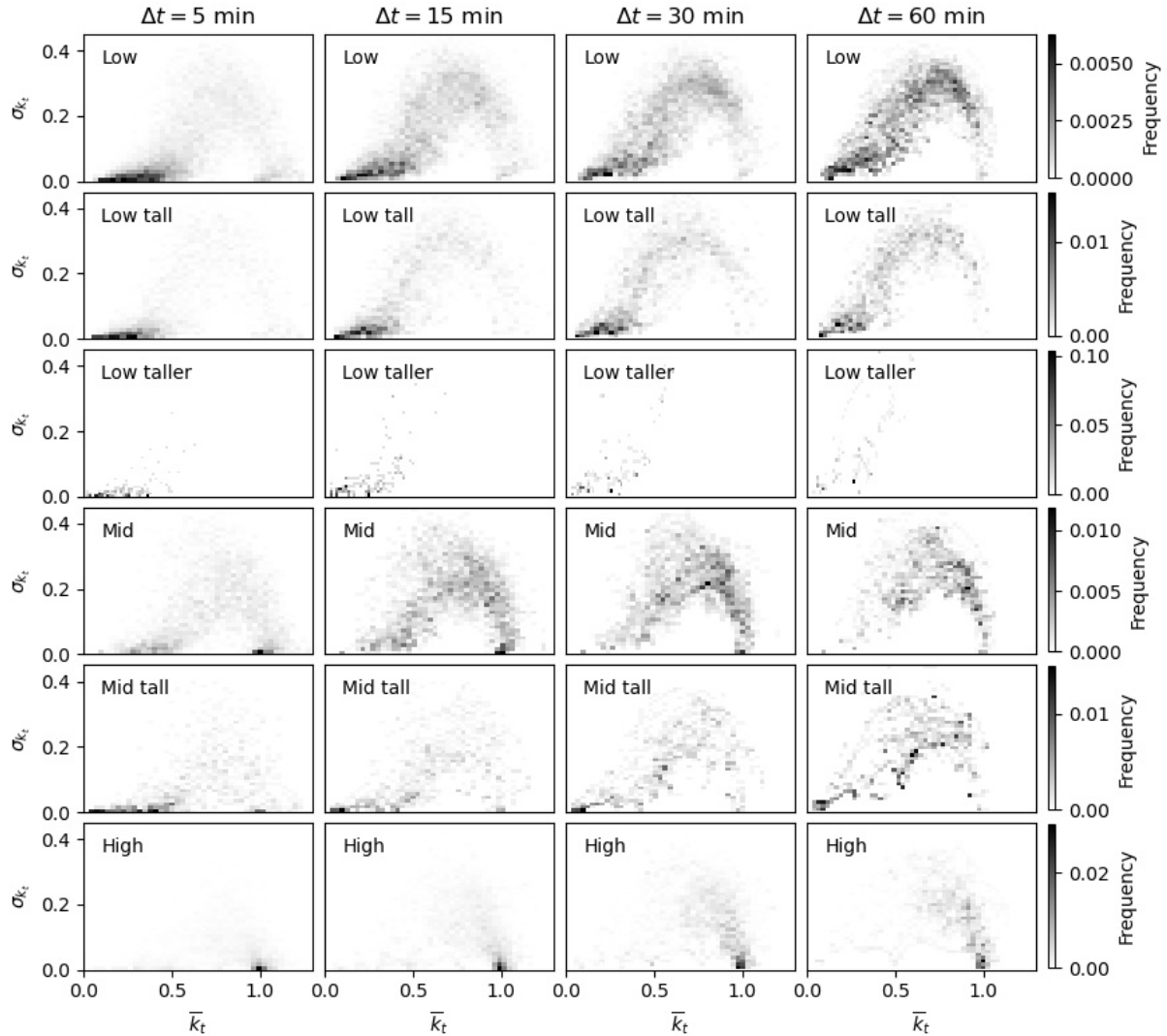


FIG. 5. Joint distributions of \bar{k}_t and σ_{k_t} by cloud type (rows) and time interval (columns).

194 a broader range in the parameter space, with 5 minute statistics peaking in the left and right bottom
 195 corners. Similarly to low clouds, the peak regions are quickly lost with longer time intervals.

196 Summarizing, hourly intervals tend to overestimate variability because quick changes can be
 197 underrepresented. This effect is observed for all types of clouds but it affects low and mid clouds
 198 more strongly. Not only variability is misrepresented but also \bar{k}_t : it can be overestimated for low
 199 and mid cloud types. From a statistical point of view, the mean overestimation of clear sky index,
 200 comparing the hourly and 1 minute values, is not found to vary greatly across cloud types (no
 201 change for high clouds and 2-18% for the rest). However, a comparison based on means only is
 202 too simplistic as it neglects the fact that the distributions are not normal, with some displaying

Dependence of sub-hourly solar variability statistics on time interval and cloud vertical position

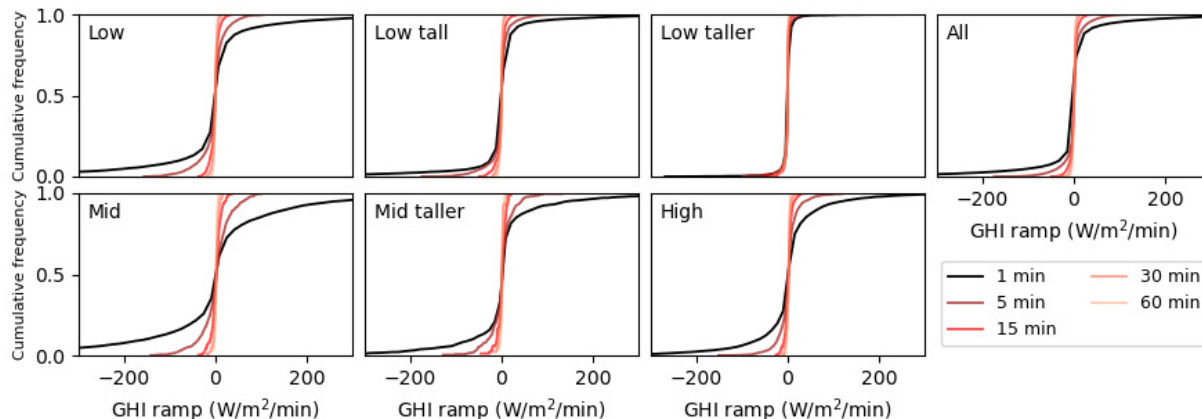


FIG. 6. Cumulative distribution of GHI ramps per cloud type and time resolution

203 a bimodal behavior (for full details of the distributions and tabulated means and medians see
 204 Appendix A).

205 D. Quantification of ramps

206 Fig. 6 shows the cumulative distribution of GHI ramps, which has been typically reported in
 207 previous studies⁶. At a first glance, both time intervals and cloud type matter. On the one hand,
 208 the effect of time is the same in all cases, longer time intervals underestimate the strength of the
 209 ramps because it smooths out the quick sub-hourly features. On the other hand, we see that the
 210 strongest ramps are linked to mid clouds, followed by mid taller, then high and low clouds.

211 We can further quantify the effect by comparing the percentiles 5 and 95, representing extreme
 212 values, shown in Table I. Longer intervals can greatly underestimate the strength of GHI ramps,
 213 with 1 minute ramps being up to 73 times stronger for mid clouds (p5), 37 times for low clouds
 214 (p95), and 31 times for high clouds (p5). The frequency of clouds and clear days at each particular
 215 site will determine the overall ramp distribution. For this case, the overall extreme ramps are 21
 216 times stronger for 1 minute intervals when compared to hourly ones.

217 IV. CONCLUSIONS AND FUTURE WORK

218 We have analyzed the sub-hourly features of solar variability and its relationship to cloud type
 219 and time intervals, using 1 minute solar data and cloud radar products from the mobile ARM
 220 campaign CACTI in Argentina. Single layer clouds were classified by their vertical position, and

Time window	All		Low		Low tall		Low taller		Mid		Mid tall		High	
	p5	p95	p5	p95	p5	p95	p5	p95	p5	p95	p5	p95	p5	p95
1 min	-95.5	93.5	-192.6	164.6	-64.8	62.4	-13.7	11.6	-286.9	261.4	-133.2	143.6	-117.0	117.6
5 min	-35.8	33.7	-57.6	40.3	-43.8	29.1	-12.9	8.3	-60.2	59.8	-50.0	42.4	-34.7	38.2
15 min	-14.5	12.5	-18.1	13.5	-18.0	11.2	-8.1	3.7	-19.8	21.1	-18.7	13.4	-13.0	14.2
30 min	-7.8	6.4	-9.4	6.3	-10.2	4.7	-12.0	2.7	-7.1	10.0	-8.0	9.9	-6.7	7.7
60 min	-4.8	4.3	-5.7	4.4	-7.2	3.3	-7.9	1.5	-3.9	5.4	-4.4	5.5	-3.7	5.2

TABLE I. Statistics of the GHI ramps in $W m^{-2} min^{-1}$, per cloud type and per time interval, where p5 and p95 correspond to percentiles 5 and 95 of the observed data.

221 time intervals of 5, 15, 30 and 60 minutes were used to compute rolling statistics of the clear sky
 222 index (the mean \bar{k}_t and the standard deviation σ_{k_t}).

223 This site shows a majority of clear conditions, followed by single clear layers. Each cloud type
 224 is associated with a different distribution of clear sky index and time of the day.

225 Solar variability was studied through the joint distribution of \bar{k}_t and σ_{k_t} , finding that the choice
 226 of time interval profoundly affects the distribution for each cloud type. Longer time windows over-
 227 estimate σ_{k_t} because they underrepresent the smaller scale dynamics, and they also overestimate \bar{k}_t
 228 for the low and mid clouds, while high clouds properties are not as affected by temporal aggrega-
 229 tion. Secondly, we quantified the change in GHI ramps with time interval and for each cloud type.
 230 The extreme values, quantified by percentiles 5 and 95, decrease with longer intervals, as expected
 231 but the effect varies per cloud type. Mid clouds generate the strongest ramps, with extreme ramps
 232 that are 71 times stronger when comparing 1 min data to hourly data. For comparison, the same
 233 ratio for all sky conditions is 19 times.

234 While this work did not resample the data to reproduce variability statistics based on hourly
 235 data, we expect those statistics to also overestimate both \bar{k}_t and σ_{k_t} , probably at higher rates since
 236 the time intervals will not be shorter than 1 h and quick changes are filtered out. As more cloud
 237 products with high resolution become available, future work should aim to improve cloud classifi-
 238 cations and other variables such as cloud optical thickness at finer time resolutions. The effects of
 239 multi layered clouds have also been left for future work, as more data would be preferred for statis-
 240 tical approaches. Finally, as the work by Riihimaki et al.⁹ has shown, solar variability forecasting
 241 should be pursued with different techniques and cloud characterization methods.

242 ACKNOWLEDGMENTS

243 MZZ thanks the Faculty of Physical and Mathematical Sciences at Universidad de Chile, for a
244 faculty incorporation grant.

245 DATA AVAILABILITY STATEMENT

246 Cloud and solar data are available at the ARM website: [https://adc.arm.gov/discovery/](https://adc.arm.gov/discovery/#/results/id::corarsclkazrbnd1kolliasM1.c1_cloud_base_best_estimate_macro_kazrarscl_)
247 [#/results/id::corarsclkazrbnd1kolliasM1.c1_cloud_base_best_estimate_macro_kazrarscl_](https://adc.arm.gov/discovery/#/results/id::corarsclkazrbnd1kolliasM1.c1_cloud_base_best_estimate_macro_kazrarscl_)
248 [cloud?dataLevel=c1&showDetails=true](https://adc.arm.gov/discovery/#/results/id::corarsclkazrbnd1kolliasM1.c1_cloud_base_best_estimate_macro_kazrarscl_) and [https://adc.arm.gov/discovery/#/results/](https://adc.arm.gov/discovery/#/results/id::corqcrad1longM1.c2_BestEstimate_down_short_hemisp_lwbroad_qcrad_radio?dataLevel=c2&showDetails=true)
249 [id::corqcrad1longM1.c2_BestEstimate_down_short_hemisp_lwbroad_qcrad_radio?dataLevel=](https://adc.arm.gov/discovery/#/results/id::corqcrad1longM1.c2_BestEstimate_down_short_hemisp_lwbroad_qcrad_radio?dataLevel=c2&showDetails=true)
250 [c2&showDetails=true](https://adc.arm.gov/discovery/#/results/id::corqcrad1longM1.c2_BestEstimate_down_short_hemisp_lwbroad_qcrad_radio?dataLevel=c2&showDetails=true), respectively. The code used in this study is available at [https://](https://github.com/mzamora/SolarVarCACTI)
251 github.com/mzamora/SolarVarCACTI.

252 Appendix A: Quantifying the overestimation of irradiance and variability

253 We have seen that for some cloud types, coarser time windows can lead to greater \bar{k}_t and σ_{k_t} . In
254 order to report the mean overestimation, we show in Fig. 7 the marginal distributions of k_t and σ_{k_t}
255 per cloud type and time window, and in Table II the corresponding mean and median values. In a
256 broad sense, we find that the mean k_t overestimation varies 2%-18% in all cloud types but the high
257 clouds, for which there is no change. Nevertheless, many distributions are not normal and even
258 bimodal and consequently, the mean values can misrepresent the changes in their distributions.
259 Complementing with the median values, these are found to vary in a broader range (3%-29%),
260 with a decrease occurring only for for high clouds, of 4%. For σ_{k_t} , the changes between 5 min and
261 hourly windows are greater, with mean / median values being at least 2 / 2.5 times greater.

262 REFERENCES

- 263 ¹P. D. Lund, J. Byrne, R. Haas, and D. Flynn, *Advances in energy systems: The large-scale*
264 *renewable energy integration challenge* (John Wiley & Sons, 2019).
- 265 ²R. Perez, M. David, T. E. Hoff, M. Jamaly, S. Kivalov, J. Kleissl, P. Lauret, M. Perez, *et al.*,
266 *Spatial and temporal variability of solar energy* (Now Publishers Incorporated, 2016).

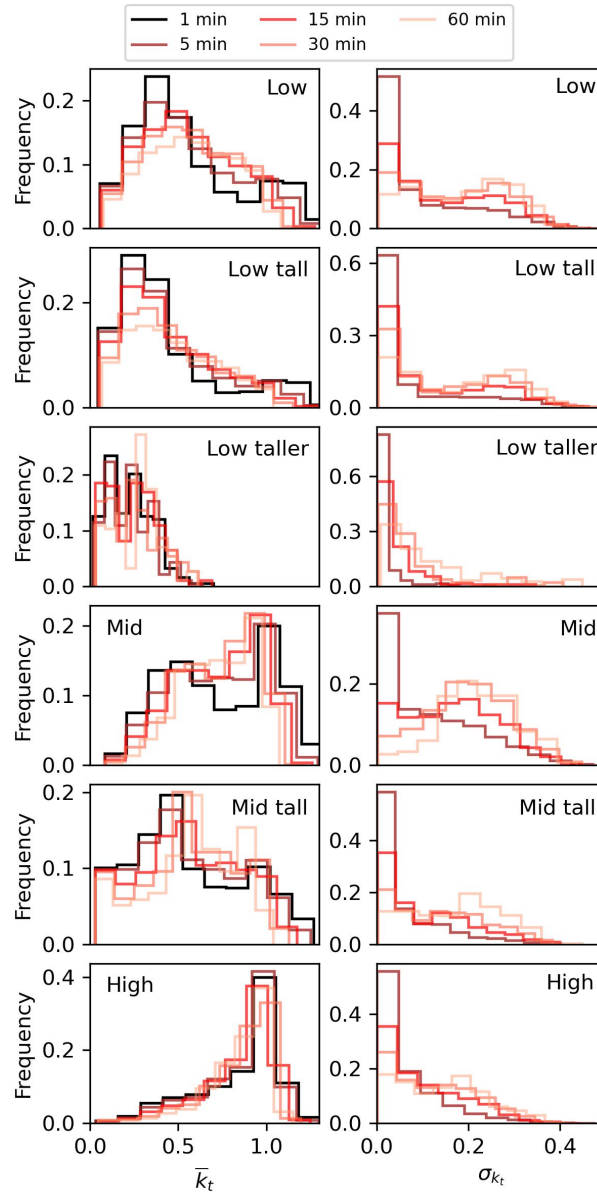


FIG. 7. Distributions of \bar{k}_t and σ_{k_t} by cloud type and time window

267 ³A. Mills and R. Wisser, “Implications of wide-area geographic diversity for short-term variability
268 of solar power,” Tech. Rep. (2010).

269 ⁴Z. K. Pecanak, F. A. Mejia, B. Kurtz, A. Evan, and J. Kleissl, “Simulating irradiance enhance-
270 ment dependence on cloud optical depth and solar zenith angle,” *Solar Energy* **136**, 675–681
271 (2016).

272 ⁵G. H. Yordanov, “A study of extreme overirradiance events for solar energy applications using
273 nasa’s i3rc monte carlo radiative transfer model,” *Solar Energy* **122**, 954–965 (2015).

Cloud type	Mean \bar{k}_t					Mean σ_{k_t}			
	1 min	5 min	15 min	30 min	1 h	5 min	15 min	30 min	1 h
Low	0.55	0.55	0.56	0.56	0.57	0.10	0.14	0.17	0.19
Low tall	0.43	0.43	0.44	0.45	0.47	0.08	0.12	0.15	0.18
Low taller	0.22	0.23	0.24	0.25	0.27	0.02	0.05	0.08	0.12
Mid	0.73	0.73	0.73	0.73	0.72	0.12	0.17	0.20	0.22
Mid tall	0.56	0.55	0.56	0.56	0.57	0.06	0.11	0.14	0.17
High	0.84	0.84	0.84	0.84	0.84	0.07	0.10	0.12	0.14

Cloud type	Median \bar{k}_t					Median σ_{k_t}			
	1 min	5 min	15 min	30 min	1 h	5 min	15 min	30 min	1 h
Low	0.46	0.50	0.53	0.55	0.56	0.04	0.12	0.16	0.20
Low tall	0.34	0.35	0.38	0.41	0.44	0.02	0.07	0.13	0.19
Low taller	0.22	0.23	0.25	0.25	0.27	0.01	0.03	0.05	0.08
Mid	0.72	0.76	0.77	0.76	0.74	0.09	0.17	0.20	0.22
Mid tall	0.49	0.51	0.54	0.56	0.60	0.03	0.07	0.14	0.19
High	0.94	0.93	0.91	0.91	0.90	0.04	0.08	0.12	0.15

 TABLE II. Mean and median values of \bar{k}_t and σ_{k_t} by cloud type and time window

- 274 ⁶L. M. Hinkelman, A. Heidinger, M. Sengupta, and A. Habte, “Relating solar resource variability
 275 to cloud type,” (2013).
- 276 ⁷M. J. Reno and J. S. Stein, “Using Cloud Classification to Model Solar Variability,” , 20 (2013).
- 277 ⁸G. M. Lohmann, A. H. Monahan, and D. Heinemann, “Local short-term variability in solar
 278 irradiance,” Atmospheric Chemistry and Physics **16**, 6365–6379 (2016).
- 279 ⁹L. D. Riihimaki, X. Li, Z. Hou, and L. K. Berg, “Improving prediction of surface solar irradiance
 280 variability by integrating observed cloud characteristics and machine learning,” Solar Energy
 281 **225**, 275–285 (2021).
- 282 ¹⁰A. Varble, S. Nesbitt, P. Salio, E. Avila, P. Borque, P. DeMott, G. McFarquhar, S. van den Heever,
 283 E. Zipser, D. Gochis, R. Houze, M. Jensen, P. Kollias, S. Kreidenweis, R. Leung, K. Rasmussen,
 284 D. Romps, C. Williams, and PNNL, BNL, ANL, ORNL, “Cloud, Aerosol, and Complex Terrain
 285 Interactions (CACTI) Field Campaign Report,” Tech. Rep. DOE/SC-ARM-19-028, 1574024
 286 (2019).

- 287 ¹¹L. Riihimaki, Y. Shi, and D. Zhang, “Data quality assessment for arm radiation data
288 (qcrad1long),”.
- 289 ¹²K. Johnson and M. Jensen, “Active remote sensing of clouds (arscl) product using ka-band arm
290 zenith radars (arsclkazrbnd1kollias),”.
- 291 ¹³P. Ineichen and R. Perez, “A new airmass independent formulation for the Linke turbidity coef-
292 ficient,” *Solar Energy* **73**, 151–157 (2002).
- 293 ¹⁴W. F. Holmgren, C. W. Hansen, and M. A. Mikofski, “pvlib python: a python package for
294 modeling solar energy systems,” *Journal of Open Source Software* **3**, 884 (2018).
- 295 ¹⁵N. Engerer and F. Mills, “Validating nine clear sky radiation models in australia,” *Solar Energy*
296 **120**, 9–24 (2015).
- 297 ¹⁶R. A. Houze, “Chapter 1 - types of clouds in earth’s atmosphere,” in *Cloud Dynamics*, Interna-
298 tional Geophysics, Vol. 104, edited by R. A. Houze (Academic Press, 2014) pp. 3–23.
- 299 ¹⁷M. Schroedter-Homscheidt, M. Kosmale, S. Jung, and J. Kleissl, “Classifying ground-measured
300 1 minute temporal variability within hourly intervals for direct normal irradiances,” *Meteorolo-
301 gische Zeitschrift* **27**, 161–179 (2018).